nature nanotechnology

ARTICLES

https://doi.org/10.1038/s41565-018-0130-2

Exploring the speed limit of toehold exchange with a cartwheeling DNA acrobat

Jieming Li[1,7], Alexander Johnson-Buck[1,2,3,4,7], Yuhe Renee Yang[5,6], William M. Shih[2,3,4], Hao Yan[5,6] and Nils G. Walter[1*]

Dynamic DNA nanotechnology has yielded nontrivial autonomous behaviours such as stimulus-guided locomotion, computation and programmable molecular assembly. Despite these successes, DNA-based nanomachines suffer from slow kinetics, requiring several minutes or longer to carry out a handful of operations. Here, we pursue the speed limit of an important class of reactions in DNA nanotechnology—toehold exchange—through the single-molecule optimization of a novel class of DNA walker that undergoes cartwheeling movements over a field of complementary oligonucleotides. After optimizing this DNA 'acrobat' for rapid movement, we measure a stepping rate constant approaching 1 s^{-1}, which is 10- to 100-fold faster than prior DNA walkers. Finally, we use single-particle tracking to demonstrate movement of the walker over hundreds of nanometres within 10 min, in quantitative agreement with predictions from stepping kinetics. These results suggest that substantial improvements in the operating rates of broad classes of DNA nanomachines utilizing strand displacement are possible.

Dynamic DNA nanotechnology exploits the programmable reconfiguration of Watson–Crick base pairing to carry out nontrivial autonomous functions inspired by both biology and macroscopic engineering, resulting in systems such as molecular walkers[1–5], assembly lines[6,7], computers[8,9] and robots[10–12]. Unlike their naturally occurring counterparts, the top-down design and transparent relationship between the sequence and function of DNA nanodevices provides rich opportunities for programmable specificity and dynamics. A fundamental process in nearly all such systems is strand displacement. This process involves the stepwise replacement of one strand of a double helix with another invading strand, a process often catalysed by short overhangs of unpaired nucleotides called toeholds[13]. A class of strand displacement reactions called toehold exchange[14] involves competition between two toeholds of similar length. Toehold exchange has found widespread use in dynamic DNA nanotechnology[8,12,15] due to its robust ability to accelerate the exchange of nearly isoenergetic DNA double helices by several orders of magnitude[14]. Indeed, toehold-mediated strand displacement reactions can have second-order rate constants in excess of 10 $M^{-1}s^{-1}$. Thus, DNA nanomachines with local effective strand concentrations in the micromolar range[16] may be able to execute individual operations in seconds or quicker if branch migration and toehold dissociation are sufficiently rapid.

Despite this theoretical rapidity, in current practice, most DNA nanomachines require several seconds to several hours to complete a single operation[6–8,17]. For instance, a recently reported cargo-sorting DNA robot utilizing toehold exchange for locomotion was found to take approximately one step every 5 min despite an only 6-nm gap between neighbouring footholds[12]. This speed is comparable with the reported speeds of other autonomous DNA walkers[10,17,18]. In one notable exception, a translocation rate of ~1 μm min^{-1} was achieved for DNA-functionalized nanoparticles, though this system utilized a burnt-bridge mechanism involving the degradation of complementary RNA strands by an external RNase H enzyme[19]. By comparison, natural protein motors have translocation rates of ~1 μm s^{-1} under saturating ATP conditions[20,21]. We hypothesized that the sluggish performance of DNA nanomachines is not due to a fundamental limitation of strand displacement reactions, but is instead the result of designs not optimized for speed.

To test this hypothesis, we designed a DNA walker with the express purpose of rapid locomotion. We then used single-molecule fluorescence resonance energy transfer (smFRET) to characterize its translocation mechanism and kinetics, and optimized its stepping rate by varying the lengths of its toehold and branch-migration domains. These optimizations resulted in stepping rate constants of more than an order of magnitude faster than existing DNA walkers. Following optimization of the design with smFRET, we used single-particle tracking to observe the movement of toehold exchange DNA walkers over distances as long as ~1 μm on a two-dimensional (2D) array of footholds. The performance of the walkers on 2D arrays was quantitatively consistent with predictions based on the stepping kinetics measured by smFRET on DNA tile substrates. This result demonstrates that this mechanism of locomotion is generalizable to different substrate types and conducive to long-range movement requiring hundreds of steps.

Design and smFRET study of a cartwheeling DNA walker

The DNA walker (Fig. 1a) was designed with speed, simplicity and robust performance as the primary objectives. Thus, we avoided the need for strand cleavage by protein or DNA enzymes because these pose the risk of creating kinetic traps for DNA walkers[22] and would prevent observations of repeated stepping. Instead, we chose a mechanism based purely on toehold exchange, which permits the walker to step an indefinite number of times between two competing foothold DNA sequences. Notably, the walker undergoes rapid sequence-guided movement over long distances while remaining

[1]Single Molecule Analysis Group, Department of Chemistry, University of Michigan, Ann Arbor, MI, USA. [2]Department of Cancer Biology, Dana Farber Cancer Institute, Boston, MA, USA. [3]Wyss Institute for Biologically Inspired Engineering, Harvard University, Boston, MA, USA. [4]Department of Biological Chemistry and Molecular Pharmacology, Harvard Medical School, Boston, MA, USA. [5]Biodesign Center for Molecular Design and Biomimetics, The Biodesign Institute, Arizona State University, Tempe, AZ, USA. [6]School of Molecular Sciences, Arizona State University, Tempe, AZ, USA. [7]These authors contributed equally: Jieming Li, Alexander Johnson-Buck. *e-mail: nwalter@umich.edu

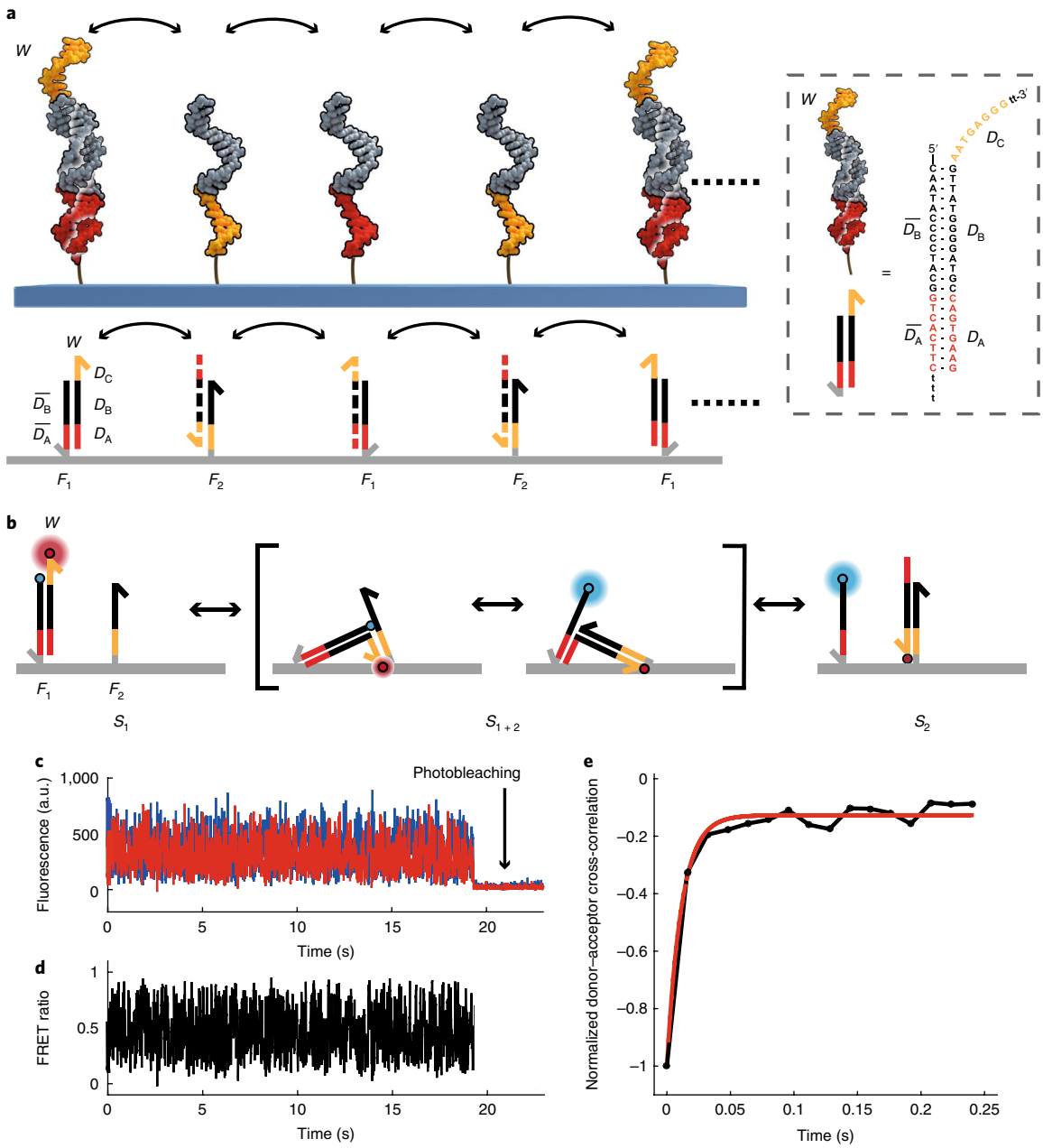

Fig. 1 | Principle and mechanism of a cartwheeling DNA walker. a, Schematic showing the intended mechanism of locomotion. **b**, Schematic of smFRET measurement of the stepping kinetics of a Cy5-labelled (red) DNA walker on a two-foothold DNA tile in which one foothold is labelled with Cy3 (blue). **c**, Rapid anticorrelated fluctuations in Cy3 (blue) and Cy5 (red) fluorescence intensity for a single walker–tile complex, suggesting branch migration in the hybrid state S_{1+2}. **d**, FRET ratio versus time for the trajectory shown in **c**. **e**, Cross-correlation analysis of the Cy3 and Cy5 signal in **c**, with a single-exponential fit indicating an anticorrelation time constant of 11.4 ms for this trajectory.

stably bound to at least one foothold at all times. Furthermore, we chose a cartwheeling mode of locomotion so that the free toehold is always distally located and can pivot about its anchor point. This design enables the walker to rapidly search for an unoccupied complement to bind, yielding comparable reaction rates for each step. As depicted in Fig. 1a, the single-stranded DNA (ssDNA) walker W undergoes head-over-heels movement over a surface of two different foothold sequences, F_1 and F_2, by toehold-mediated strand displacement. The two foothold sequences comprise a common middle branch migration domain $\overline{D_B}$ and toehold domains $\overline{D_A}$ and $\overline{D_C}$, which are unique to each foothold sequence. The walker is complementary to all three domains, with nearly identical free energy of hybridization to $\overline{D_A}$ and $\overline{D_C}$. Thus, in a field of both F_1 and F_2, the walker is expected to alternate between binding to each of the footholds, resulting in an indefinite number of steps over the field of footholds.

To mechanistically characterize and optimize the stepping behaviour of the transporter, we began with a simple DNA tile system bearing two adjacent footholds for the walker to step between. This two-foothold system consists of a four-helix DNA tile decorated with ssDNA overhangs F_1 and F_2 as well as a biotin label for surface immobilization in total internal reflection fluorescence (TIRF) measurements (see Supplementary Methods and Supplementary Figs. 1–3). The footholds are spaced by ~7 nm to match the 17–21 nucleotide length of the duplex formed by the binding of the walker to a foothold and equipped with $(dT)_3$

linkers to provide conformational flexibility. The DNA walker $W_{a\_b\_c}$ consists of a middle branch migration domain D_B of length b (generally 13 nucleotides) flanked by two toehold domains D_A and D_C (Supplementary Fig. 1) with lengths a and c ($a=c=5$–8 nucleotides). The sequence of the walker was chosen to allow for comparison with prior studies of toehold exchange kinetics[14]. To permit measurement of stepping kinetics by smFRET[23,24], the 5′-end of F_1 is labelled with the FRET donor Cy3, and the 3′-end of $W_{a\_b\_c}$ is labelled with the FRET acceptor Cy5. Thus, any stepping of W between F_1 and F_2 through toehold exchange is expected to give rise to a time-dependent change in FRET efficiency between Cy3 and Cy5 (Fig. 1b). To reduce the likelihood of analysing multiple walkers bound to one DNA tile, we combined the walker with a 1.5-fold molar excess of DNA tile, and our smFRET analysis filtered out complexes with >1 photobleaching step in the donor or acceptor channel.

First, we characterized by smFRET the behaviour of a walker bearing 8-nucleotide toehold domains ($W_{8\_13\_8}$). Less than 30% of walkers exhibited static high- or low-FRET efficiency behaviour, which may result from only one of the footholds being present or accessible. However, the largest fraction of walkers (60–70%) exhibited a FRET efficiency varying between 0.3 and 0.7 (Fig. 1c,d). On close inspection, this mid-FRET state contained rapid anticorrelated fluctuations of Cy3 and Cy5 fluorescence intensity, indicating rapid changes in the distance between Cy3 and Cy5 (Fig. 1e). The cross-correlation function between Cy3 and Cy5 decays with a time constant of 12 ± 3 ms. These fluctuations were rapid in nature and the apparent FRET efficiency occupied a continuum of values rather than discrete states. Thus, we hypothesized that these fluctuations are predominantly due to reversible branch migration of domain D_B, with only transient dissociation of either toehold from its respective foothold strand. That is, instead of occupying either state S_1 or S_2 (Fig. 1b), the walker exists primarily in a hybrid dynamic equilibrium state S_{1+2} in which it is partially base-paired to both F_1 and F_2. This result is consistent with expectations based on the local effective concentration of 250 μM measured in a similar tile-based system[16], whereby the equilibrium is expected to strongly favour hybridization of the 8-nucleotide toehold sequences. The toehold-dissociated states S_1 and S_2 are not typically observed because of their low occupancy and short lifetimes. Changing the toehold length to 7, 6 or 5 nucleotides produced a similar kinetic behaviour, consistent with the presence of the same branch migration domain length $b=13$ (Supplementary Fig. 4). Monte Carlo simulations of branch migration within a 13-nucleotide domain (Supplementary Note 1 and Supplementary Fig. 5) suggest that an anticorrelation time constant of ~12 ms will occur when the lifetime of an individual base pair step along the duplex is ~100 μs. This result is similar to previous estimates based on kinetic modelling from bulk fluorescence measurements[25] and from three-stranded branch migration of genomic-length DNA sequences[26,27].

To further test our hypothesis of a hybrid S_{1+2} state, a third foothold strand F_1' with the same sequence as F_1 was added to assemble a three-foothold DNA tile (Supplementary Figs. 1 and 6). The addition of this third foothold is expected to enable the walker to occupy a second hybrid state $S_{2+1'}$ (Fig. 2a), resulting in a new low-FRET state in addition to the mid-FRET state observed for the two-foothold system. Indeed, most mid-FRET trajectories for $W_{8\_13\_8}$ showed slow transitions to and from an additional FRET state of ~0.3 on the three-foothold tile (Fig. 2b), suggesting a new, slower process limited by toehold dissociation. Based on these results, we predicted that decreasing the length of the toehold would yield dramatically faster stepping behaviours of walkers, since the rate of dissociation of short DNA duplexes increases exponentially with decreasing length[28,29]. Indeed, walkers with 7-, 6- or 5-nucleotide toeholds showed two-state FRET behaviours with much more rapid transitions between states (Fig. 2b–i). The median lifetimes (calculated from the per-molecule mean of both high- and low-FRET state lifetimes) decreased from 31.3 s (interquartile range (IQR) 52.1–16.5 s) for $W_{8\_13\_8}$ to 1.4 s (IQR 3.7–1.1 s) for $W_{5\_13\_5}$, yielding rate constants of stepping between 0.03 and 0.72 s^{-1} (Fig. 2n). Given the step size of 7 nm, the fastest walker exhibited an average (undirected) translocation speed of ~300 nm min^{-1}. While the stepping rate increased by more than an order of magnitude when the toehold length was decreased to 7 nucleotides, further increases where marginal, and the apparent stepping rate of $W_{5\_13\_5}$ was very similar to that of $W_{6\_13\_6}$. In contrast, kinetic Monte Carlo simulations of stepping on a three-foothold tile predicted an exponential decrease in the stepping time as a function of toehold length, in direct proportion to the toehold dissociation rate constants (Supplementary Note 1, Supplementary Fig. 5). One possible explanation for this discrepancy is that as toehold nucleotides are removed from the walker, base pairs in the rigid walker–foothold duplex are replaced by unpaired nucleotides near the base of the foothold. This process may influence binding and/or dissociation kinetics of toehold D_A by virtue of the much smaller persistence length of ssDNA[30]. For example, if the topology of the DNA tile positions F_2 at slightly different distances from F_1 and F_1', the replacement of duplex with single-stranded DNA may result in different binding rates of toehold D_A to F_1 and F_1'. Our simulations suggest that such an asymmetry, combined with the finite time resolution of our measurements, could yield measured dwell times that deviate from the predicted exponential dependence in a manner consistent with our smFRET observations (Supplementary Note 1, Supplementary Fig. 5). This deviation occurs because a toehold D_A may dissociate from, and re-associate with, F_1 several times before binding to F_1'. This effect gives the appearance of a single long-lived high-FRET state because the unbound state of the toehold is too short to resolve experimentally. Consistent with this hypothesis, smFRET measurements did reveal an increasing bias towards high-FRET states as the toehold length decreased (Fig. 2b–e,n), a bias that was intriguingly reversed when the DNA tile was replaced by a DNA origami substrate. In addition, as the length of the toeholds decreased, the difference in apparent FRET efficiency between the two main states increased (Fig. 2j–m). This observation is consistent with the expected decrease in the distance between the donor and acceptor dyes in the S_{1+2} state, as well as an increase in the donor–acceptor distance in the $S_{2+1'}$ state, when a shorter toehold is present.

To investigate the role of branch migration in the stepping kinetics of walkers with shorter toeholds, we performed smFRET measurements on walkers with different lengths of domain D_B, with accompanying changes in the foothold sequences to maintain complementarity with each walker. As with previous walker designs, smFRET transitions were observed for $W_{6\_6\_6}$ and $W_{6\_20\_6}$ (Supplementary Fig. 7). Kinetic Monte Carlo simulations predicted that stepping dwell times will increase linearly in proportion to the length of D_B, since walkers will spend more time in branch migration intermediates from which toehold dissociation is difficult or impossible (Supplementary Note 1). Indeed, when the middle domain increased to 20 nucleotides (walker $W_{6\_20\_6}$), the median stepping lifetime was 2.7 s (IQR 8.7–1.4 s), which is slightly longer than that of $W_{6\_13\_6}$ (1.6 s, IQR 8.7–1.1 s). However, when D_B was decreased to 6 nucleotides (walker $W_{6\_6\_6}$), the median stepping lifetime increased to 23.6 s (IQR 39.4–5.2) (Fig. 2o). This result was contrary to the predictions of a simple branch migration model, suggesting that the structural details of the walker–tile complex (such as the match between walker length and foothold spacing) may play a role. The $(dT)_3$ ssDNA spacers between the foothold strands and the tile are expected to provide sufficient flexibility to compensate for the difference of ± 2.3 nm from the addition or subtraction of 7 nucleotides from D_B. However, altering the length of the branch migration domain may still introduce an incongruity between the reach

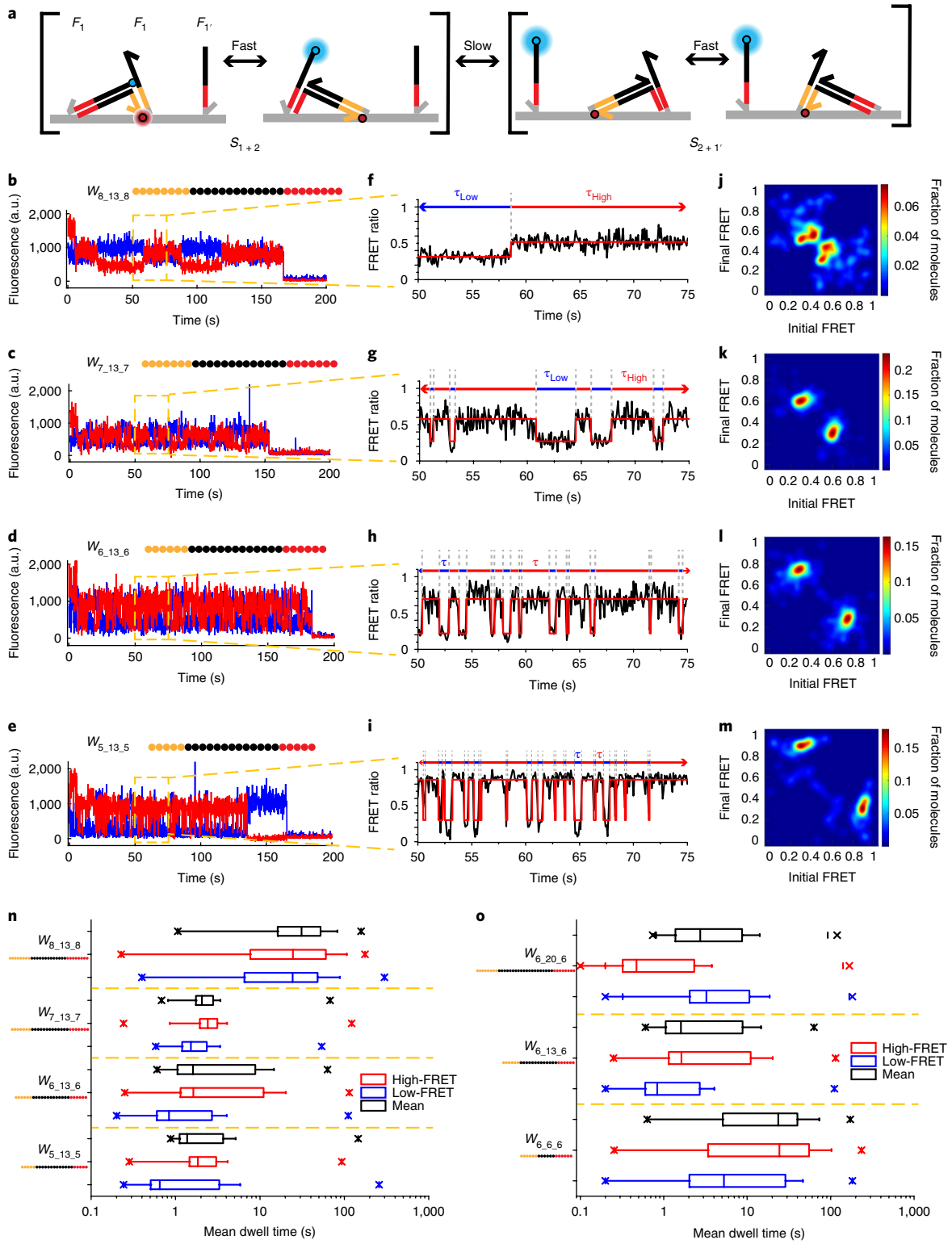

Fig. 2 | Single-molecule FRET characterization of walkers with varying toehold lengths. a, Kinetic model of stepping and associated FRET transitions for a Cy5-labelled (red) DNA walker on a Cy3-labelled (blue) three-foothold DNA tile. **b**–**e**, Representative smFRET trajectories of walkers with varying toehold lengths on a three-foothold DNA tile. Cy3 fluorescence is shown in blue, while Cy5 fluorescence is shown in red. The elevated Cy5 signal in the first ~10 s of each trace results from direct excitation at 640 nm to confirm the presence of an active acceptor on each walker–tile complex. **f**–**i**, Zoomed-in trajectories showing FRET transitions for 25-s segments of the molecules depicted in **b**–**e**. **j**–**m**, Transition occupancy density plots illustrating the most common FRET transitions for each walker. $N = 87$, 96, 107 and 109 for $W_{5\_13\_5}$, $W_{6\_13\_6}$, $W_{7\_13\_7}$ and $W_{8\_13\_8}$, respectively. **n**, Box-and-whisker plot of stepping kinetics in the high- and low-FRET states for walkers with varying toehold domain (D_A and D_C) lengths. **o**, Box-and-whisker plot for walkers with varying middle domain (D_B) lengths. $N = 105$ and 132 for $W_{6\_6\_6}$ and $W_{6\_20\_6}$, respectively. The box includes the population of all molecules from the 25th percentile to 75th percentile; whiskers correspond to 0 and 100th percentiles, excluding outliers. Crosses denote the lower and upper bounds, inclusive of outliers.

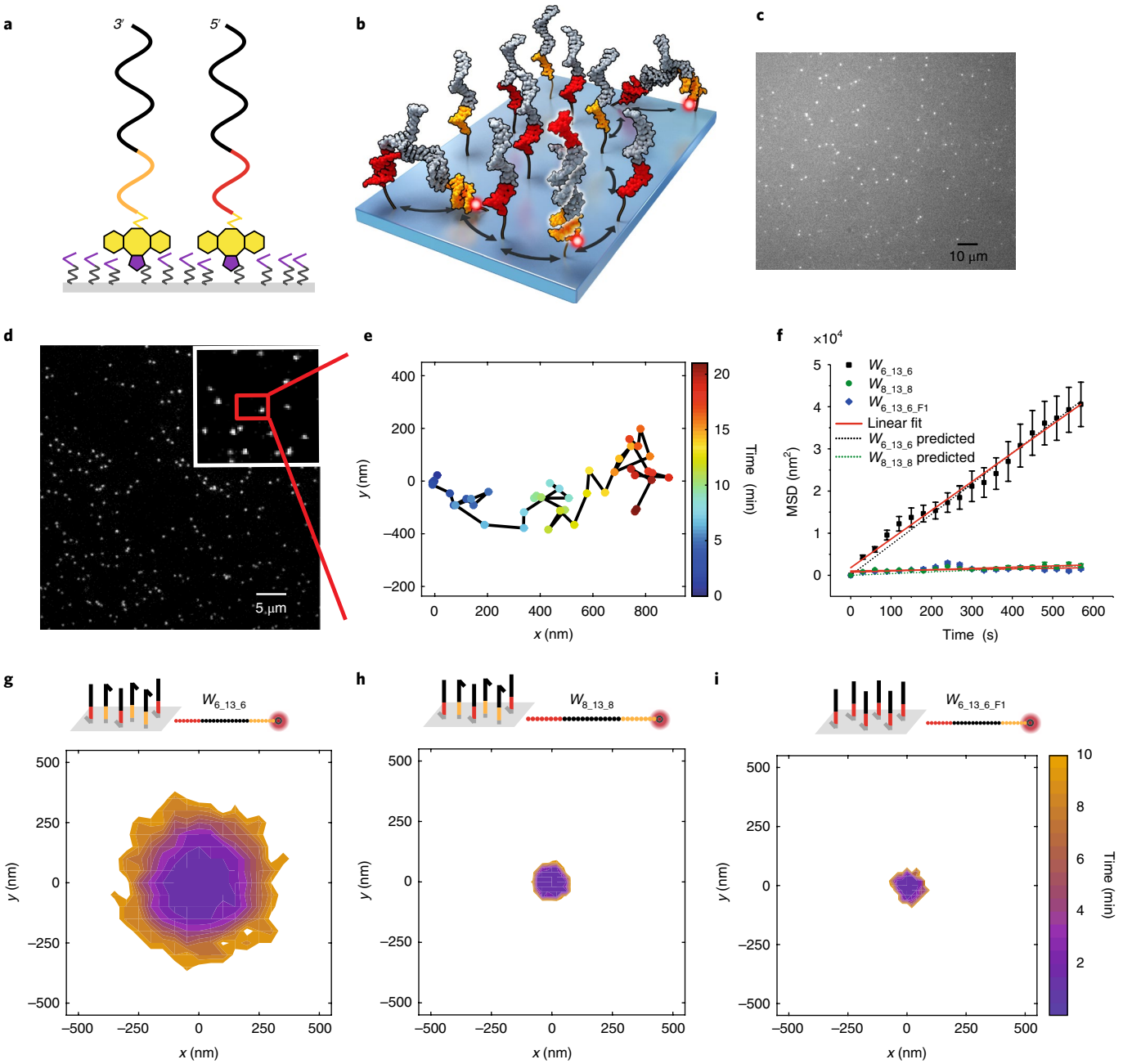

Fig. 3 | Characterization of 2D foothold arrays and long-range walker movement. a, Schematic of F_1 and F_2 DNA conjugated to a glass coverslip surface at high density via copper-free click chemistry. Surface azides are shown in purple and dibenzocyclooctyne (DBCO) in yellow. **b**, Schematic of walker movement over a 2D array of footholds. **c**, TIRF image of complementary oligonucleotides bound to footholds on a coverslip surface at a ratio of 1 fluorescently labelled oligonucleotide:1 million unlabelled fluorescent oligonucleotides. **d**,**e**, TIRF image of Cy5-labelled $W_{6\_13\_6}$ on a quartz slide coated with F_1 and F_2 (**d**) and a representative fast-moving trajectory of $W_{6\_13\_6}$ (**e**). **f**, Mean square displacement (MSD) versus time plot for $W_{6\_13\_6}$, $W_{8\_13\_8}$ and $W_{6\_13\_6\_F1}$ (control with F_1 only). Error bars represent one standard deviation. The diffusion coefficients derived from linear regression fits to the MSD versus time data are 17, 2.3 and 0.33 $nm^2 s^{-1}$, respectively. The MSD curves predicted from the stepping kinetics measured by smFRET on DNA tiles (broken lines in green and black) are also shown for comparison. **g**–**i**, Comparison of the extent of diffusion (region comprising 95% of trajectories, with all starting at the origin) of $W_{6\_13\_6}$, $W_{8\_13\_8}$ and $W_{6\_13\_6\_F1}$ (control with F_1 only) over a 10-min period of observation.

of the walker and the spacing between foothold strands, since the distance between adjacent foothold strands is fixed at ~7 nm. In any case, the lack of a positive correlation between the length of D_B and the stepping lifetime suggests that any impact of branch migration on the stepping rate for values of b between 6 and 20 nucleotides is overshadowed by other factors. Such factors include toehold binding and dissociation kinetics and the match between walker length and foothold spacing.

Longer-range walker movement on 2D foothold arrays

Based on smFRET measurements, the DNA walker with the fastest stepping rate and most homogeneous behaviour was $W_{6\_13\_6}$. To test the performance of this optimized DNA walker as a long-distance 2D transporter, we developed a surface modification method that yields a high density of DNA footholds on a glass coverslip. In this method, alkyne-functionalized F_1 and F_2 are attached to an azide-modified coverslip through copper-free click chemistry. This process

results in random, high-density conjugation of the two different foothold strands to the surface (Fig. 3a,b; see Methods). Using TIRF microscopy, we measured an average oligonucleotide surface density of $1.67 \times 10^4\,\mu m^{-2}$. This density is predicted to yield distances between nearest-neighbour F_1 and F_2 strands varying from ~2 to 13 nm, assuming a completely random distribution of footholds on the slide surface (Fig. 3c, Supplementary Fig. 8 and Methods). This estimate should be interpreted as an upper bound on the average spacing between footholds, since our measurements may underestimate the true density if a significant fraction of probe fluorophores are photobleached prior to the measurement. To confirm that larger inter-foothold distances are compatible with rapid stepping by the walker, we repeated our smFRET measurements of stepping in a three-foothold system constructed from a distinct DNA origami scaffold (Supplementary Fig. 9, Supplementary Table 1). In addition, a dT_6 linker instead of a dT_3 linker between the footholds and the origami was used for added flexibility. Despite the larger distance between adjacent foothold sites on this DNA origami (~10.5 nm on average, assuming 0.332 nm per nucleotide) compared with the previous tile system (~7 nm), smFRET characterization revealed a similar stepping rate constant of ~0.5 s^{-1} (IQR 0.6–0.1 s^{-1}) for $W_{6\_13\_6}$ on this new scaffold. This result suggests that the stepping rate is robust against small perturbations in foothold spacing.

Next, we characterized the long-range movement of the optimized walker $W_{6\_13\_6}$ by 2D single-particle tracking using TIRF microscopy (Fig. 3d,e). Most of the molecules travelled > 200 nm from their starting position within 10 min (Fig. 3f), resulting in a measured 2D diffusion coefficient of $17 \pm 0.5\,nm^2\,s^{-1}$ ($R^2 = 0.99$). Some molecules were observed to travel nearly 1 µm before photobleaching (Fig. 3d; see Supplementary Fig. 10 for other trajectories of this walker). In contrast, particle tracking of $W_{8\_13\_8}$ indicated a much smaller diffusion coefficient of $0.7 \pm 0.1\ nm^2\,s^{-1}$ ($R^2 = 0.73$) (Fig. 3f,h), or $2.2 \pm 0.2\,nm^2\,s^{-1}$ ($R^2 = 0.89$) if a single extremely fast-moving outlier is included (Supplementary Fig. 11). This result was consistent with predictions based on its ~10-fold slower stepping rate as measured by smFRET. For comparison, a random walk model with predicted step sizes of 10.8 and 11.1 nm for $W_{6\_13\_6}$ and $W_{8\_13\_8}$, respectively (see Methods and Supplementary Fig. 8), and stepping rates taken from smFRET measurements on three-foothold DNA tiles predicted diffusion coefficients of $18.1\,nm^2\,s^{-1}$ and $0.99\,nm^2\,s^{-1}$ for $W_{6\_13\_6}$ and $W_{8\_13\_8}$, respectively. This close agreement with the predictions suggests that the optimized walker functions as designed, even on a different substrate and over substantially longer distances. Moreover, a surface with only a single foothold type (F_1) resulted in insignificant diffusion of $W_{6\_13\_6}$ (D ~$0.33 \pm 0.20\,nm^2\,s^{-1}$ ($R^2 = 0.09$), standard deviations in position $\sigma_x = 16.4$ nm, $\sigma_y = 15.2$ nm), consistent with the designed walking mechanism involving both footholds (Fig. 3f,i; Supplementary Fig. 12).

Conclusions

We created a new class of ssDNA walker that exploits a toehold exchange mechanism to traverse arrays of specific oligonucleotide sequences in a cartwheeling fashion. The directionally unbiased movement of the walker has useful precedents in both nature and nanotechnology. For example, the kinesin MCAK utilizes undirected, one-dimensional diffusion to rapidly locate the ends of microtubules for depolymerization, resulting in faster searching over short distances than would be possible with direct binding from solution[31]. In the field of nanotechnology, synthetic biochemical cascades have exploited undirected, two-way transport to promote reagent channelling between coupled enzymes using a swinging arm over short distances (~10 nm)[16]. Moreover, a cargo-sorting robot was recently reported to use unbiased diffusion to transfer payloads over distances of tens of nanometres in a period of hours[12]. It is likely that the cartwheeling mode of locomotion of the DNA acrobat plays an important role in generating the rapid stepping relative to similar systems studied previously, since some of these employed similar domain lengths and yet still exhibited stepping orders of magnitude slower than our system[12]. One advantage of the cartwheeling geometry is that a rigid double-stranded segment always bridges between adjacent footholds, ensuring rapid toehold binding if there is a good match between the walker length and foothold spacing. Second, it has been suggested that the cargo-sorting robot may exhibit slow branch migration when strand displacement is initiated at the distal end of a foothold and proceeds towards the surface due to the entropic cost of stretching the ssDNA away from the surface[12]. If this suggestion is true, the DNA acrobat overcomes this issue by virtue of the fact that branch migration always proceeds away from the point of attachment. Also of note is that most of our DNA acrobat designs remain bound to their footholds at all times by at least 18 nucleotides. This result indicates that they should be highly processive at room temperature, a prediction that is consistent with our single-particle tracking measurements, which suggest that the $W_{6\_13\_6}$ walker may take hundreds of steps without dissociating.

The present study of a cartwheeling DNA walker also shows that the speed and range of similar DNA-based systems may be improved with careful optimization. The fastest of our toehold exchange walkers can search among ~43 foothold sites per minute with a stepping distance of ~10 nm. While still much slower than many natural motor proteins (for example, $0.38\,\mu m^2\,s^{-1}$ for MCAK[31]), the stepping rate of this cartwheeling walker is more than an order of magnitude higher than that of other DNA-only walker systems. This improvement in performance was enabled by detailed single-molecule analyses of stepping kinetics as a function of key design parameters, an approach that is likely to be generalizable to many other systems in nanotechnology. While decreasing the toehold length from 8 to 5 nucleotides yields faster stepping rates as predicted, the marginal improvements in stepping rate appear to diminish below ~6 nucleotides, in contrast to the predictions of our kinetic modelling. These results, as well as those for the shortened walker $W_{6\_6\_6}$, suggest that optimizing the mechanical properties of the system (for example, the reach of the walker and the entropic tension in single-stranded linker segments) may also be important, and could yield further improvements.

Finally, the present characterization of toehold exchange reactions at very high local effective reagent concentrations in a variety of contexts suggests that it may be challenging to obtain rate constants significantly faster than $1\,s^{-1}$ for conventional strand displacement operations in DNA nanomachines. To surpass this apparent speed limit, dynamic DNA nanotechnology may need to incorporate further innovations inspired by natural systems, such as more precise control of local DNA mechanics and conformational changes, as well as judicious coupling to (rapid) exergonic processes.

Methods

Methods, including statements of data availability and any associated accession codes and references, are available at https://doi.org/10.1038/s41565-018-0130-2.

Received: 6 October 2017; Accepted: 29 March 2018;
Published online: 7 May 2018

References

1. Sherman, W. B. & Seeman, N. C. A precisely controlled DNA biped walking device. *Nano Lett.* **4**, 1203–1207 (2004).
2. Shin, J.-S. & Pierce, N. A. A synthetic DNA walker for molecular transport. *J. Am. Chem. Soc.* **126**, 10834–10835 (2004).
3. Tian, Y., He, Y., Chen, Y., Yin, P. & Mao, C. A DNAzyme that walks processively and autonomously along a one-dimensional track. *Angew. Chem. Int. Ed. Engl.* **44**, 4355–4358 (2005).
4. Bath, J., Green, S. J. & Turberfield, A. J. A free-running DNA motor powered by a nicking enzyme. *Angew. Chem. Int. Ed. Engl.* **44**, 4358–4361 (2005).

5. Omabegho, T., Sha, R. & Seeman, N. C. A bipedal DNA Brownian motor with coordinated legs. *Science* **324**, 67–71 (2009).
6. Gu, H., Chao, J., Xiao, S.-J. & Seeman, N. C. A proximity-based programmable DNA nanoscale assembly line. *Nature* **465**, 202–205 (2010).
7. He, Y. & Liu, D. R. Autonomous multistep organic synthesis in a single isothermal solution mediated by a DNA walker. *Nat. Nanotech.* **5**, 778–782 (2010).
8. Qian, L. & Winfree, E. Scaling up digital circuit computation with DNA strand displacement cascades. *Science* **332**, 1196–1201 (2011).
9. Qian, L., Winfree, E. & Bruck, J. Neural network computation with DNA strand displacement cascades. *Nature* **475**, 368–372 (2011).
10. Lund, K. et al. Molecular robots guided by prescriptive landscapes. *Nature* **465**, 206–210 (2010).
11. Douglas, S. M., Bachelet, I. & Church, G. M. A logic-gated nanorobot for targeted transport of molecular payloads. *Science* **335**, 831–834 (2012).
12. Thubagere, A. J. et al. A cargo-sorting DNA robot. *Science* **357**, eaan6558 (2017).
13. Zhang, D. Y. & Seelig, G. Dynamic DNA nanotechnology using strand-displacement reactions. *Nat. Chem.* **3**, 103–113 (2011).
14. Zhang, D. Y. & Winfree, E. Control of DNA strand displacement kinetics using toehold exchange. *J. Am. Chem. Soc.* **131**, 17303–17314 (2009).
15. Zhang, D. Y., Chen, S. X. & Yin, P. Optimizing the specificity of nucleic acid hybridization. *Nat. Chem.* **4**, 208–214 (2012).
16. Fu, J. et al. Multi-enzyme complexes on DNA scaffolds capable of substrate channelling with an artificial swinging arm. *Nat. Nanotech.* **9**, 531–536 (2014).
17. Wickham, S. F. J. et al. Direct observation of stepwise movement of a synthetic molecular transporter. *Nat. Nanotech.* **6**, 166–169 (2011).
18. Cha, T.-G. et al. A synthetic DNA motor that transports nanoparticles along carbon nanotubes. *Nat. Nanotech.* **9**, 39–43 (2014).
19. Yehl, K. et al. High-speed DNA-based rolling motors powered by RNase H. *Nat. Nanotech.* **11**, 184–190 (2015).
20. King, S. J. & Schroer, T. A. Dynactin increases the processivity of the cytoplasmic dynein motor. *Nat. Cell Biol.* **2**, 20–24 (2000).
21. Kural, C. et al. Kinesin and dynein move a peroxisome in vivo: a tug-of-war or coordinated movement? *Science* **308**, 1469–1472 (2005).
22. Pan, J., Li, F., Cha, T.-G., Chen, H. & Choi, J. H. Recent progress on DNA based walkers. *Curr. Opin. Biotechnol.* **34**, 56–64 (2015).
23. Roy, R., Hohng, S. & Ha, T. A practical guide to single-molecule FRET. *Nat. Methods* **5**, 507–516 (2008).
24. Walter, N. G., Huang, C.-Y., Manzo, A. J. & Sobhy, M. A. Do-it-yourself guide: how to use the modern single-molecule toolkit. *Nat. Methods* **5**, 475–489 (2008).
25. Srinivas, N. et al. On the biophysics and kinetics of toehold-mediated DNA strand displacement. *Nucleic Acids Res.* **41**, 10641–10658 (2013).
26. Panyutin, I. G. & Hsieh, P. Formation of a single base mismatch impedes spontaneous DNA branch migration. *J. Mol. Biol.* **230**, 413–424 (1993).
27. Beattie, K. L., Wiegand, R. C. & Radding, C. M. Uptake of homologous single-stranded fragments by superhelical DNA. *J. Mol. Biol.* **116**, 783–803 (1977).
28. Jungmann, R. et al. Single-molecule kinetics and super-resolution microscopy by fluorescence imaging of transient binding on DNA origami. *Nano Lett.* **10**, 4756–4761 (2010).
29. Dupuis, N. F., Holmstrom, E. D. & Nesbitt, D. J. Single-molecule kinetics reveal cation-promoted DNA duplex formation through ordering of single-stranded helices. *Biophys. J.* **105**, 756–766 (2013).
30. Smith, S. B., Cui, Y. & Bustamante, C. Overstretching B-DNA: the elastic response of individual double-stranded and single-stranded DNA molecules. *Science* **271**, 795–799 (1996).
31. Helenius, J., Brouhard, G., Kalaidzidis, Y., Diez, S. & Howard, J. The depolymerizing kinesin MCAK uses lattice diffusion to rapidly target microtubule ends. *Nature* **441**, 115–119 (2006).

Acknowledgements

This work was supported primarily by the US Department of Defense Army Research Office MURI award W911NF-12-1-0420 to N.G.W. and H.Y. The authors thank J. Damon Hoff for technical support, Z. R. Li for graphic design support, and B. Nijholt, E. Krieg, A. M. Bergman and W. Benjamin Rogers for discussions about DNA origami design.

Author contributions

A.J.-B. conceived the ideas. Y.R.Y. designed, fabricated and characterized the DNA tile samples. W.M.S. and A.J.-B. designed, fabricated and characterized the DNA origami samples. J.L. and A.J.-B. performed smFRET and single-particle tracking measurements. J.L., A.J.-B., and N.G.W. analysed and interpreted the data. J.L. and A.J.-B. co-wrote the paper, and all authors discussed the results and edited the manuscript.

Competing interests

The authors declare no competing interests.

Additional information

Supplementary information is available for this paper at https://doi.org/10.1038/s41565-018-0130-2.

Reprints and permissions information is available at www.nature.com/reprints.

Correspondence and requests for materials should be addressed to N.G.W.

Publisher's note: Springer Nature remains neutral with regard to jurisdictional claims in published maps and institutional affiliations.

Methods

Materials. Single-stranded oligonucleotides, Cy3- and Cy5-labelled oligonucleotides and amine-modified oligonucleotides were purchased from Integrated DNA Technologies. Dye-labelled oligonucleotides were HPLC-purified by the manufacturer. Streptavidin (S-888), biotinylated bovine serum albumin (bBSA, 29130), Trolox (218940050) and 3,4-dihydroxybenzoic acid (AC114891000) were purchased from Thermo Fisher Scientific. Protocatechuate 3,4-dioxygenase, Tris base, acetic acid, EDTA, magnesium acetate, dibenzocyclooctyne-*N*-hydroxysuccinimidyl ester (761524), 11-azidoundecyltriethoxysilane (SIK4711-30), *N*,*N*-dimethylformamide (DMF), triethylamine (TEA) and sodium acetate were purchased from Sigma-Aldrich.

Design, assembly and characterization of four-helix DNA tiles. The detailed sequence designs of the four-helix DNA tile nanostructures are shown in Supplementary Figs. 1 and 2. The computer program Tiamat was used for structural design and sequence generation. Oligonucleotides were purified using 6–8% denaturing polyacrylamide gel electrophoresis (PAGE) at room temperature. The bands corresponding to the correct strand length were imaged using a UV lamp (254 nm) and then cut from the gel, chopped into small pieces and incubated overnight in elution buffer (500 mM ammonium acetate, 10 mM magnesium acetate, 2 mM sodium ethylenediaminetetraacetic acid, pH 8.0). The DNA strands were extracted from the gel pieces by centrifugation using a Costar Spin X filtration device (Corning, cellulose acetate membrane with 0.22 µm size). The filtrate was then ethanol precipitated, washed using ethanol and dried under vacuum. The DNA strands were dissolved in nanopure water and the concentrations of the individual purified strands were measured by UV absorbance at 260 nm using the extinction coefficient provided by the manufacturer.

The DNA strands constituting each DNA structure were mixed in 1× TAE-Mg^{2+} buffer (40 mM Tris, 20 mM acetic acid, 2 mM EDTA and 12.5 mM magnesium acetate, pH 8.0) to reach a final concentration of 1 µM per strand. All samples were annealed using an Eppendorf Mastercycler using the following annealing protocol: heat to 90 °C; cool from 90 °C to 72 °C over 10 min; then from 68 °C °C to 24 °C over 60 min; and finally holding at 15 °C.

The formation of the DNA structures was characterized by native PAGE. Native PAGE gels (5%) were prepared at room temperature and run for 4–6 h at a constant voltage of 200 V. Cy3-labelled structures were visualized using a UV lamp (365 nm) and then cut from the gel, chopped into small pieces and incubated overnight in 1× TAE-Mg^{2+} buffer. The DNA structures were then extracted from the gel pieces by centrifugation using a Costar Spin X filtration device (Corning, cellulose acetate membrane with 0.22 µm size). For analytical native PAGE, the gel was subsequently stained with SYBR Green/Gold.

Design, fabrication and characterization of DNA origami. The DNA origami structure was built on a square helical lattice using the program caDNAno, and staple strand sequences (Supplementary Table 1) were designed to be complementary to a contiguous segment of the M13 p7308 scaffold sequence. Assembly was performed by combining 10 nM of the p7308 scaffold with a tenfold molar excess of all staple sequences in TE buffer with 10 mM $MgCl_2$, then performing the following annealing protocol on a Tetrad 2 Peltier thermal cycler: heat to 80 °C; decrease to 60 °C over 70 min; decrease from 60 °C to 24 °C over 66 h; and then hold at 4 °C. Origami structures were purified from excess staples by 2% agarose gel electrophoresis in 0.5× TBE + 10 mM $MgCl_2$. The gel was scanned using a Typhoon FLA 9000 (GE Healthcare Life Sciences), and a scale printout was laid under the gel to permit excision of the origami bands. Origami structures were eluted from the gel by centrifugation for 5 min at 5,000 × *g* in Freeze 'N Squeeze spin columns (Bio-Rad). Recovery was confirmed by again running the purified origami structures on a 2% agarose gel and scanning for Cy3 fluorescence. DNA origami morphology was characterized by negative-stain transmission electron microscopy (TEM) using a JEOL 1400 TEM after depositing origami (3 µl) on a plasma-treated carbon Formvar grid (Electron Microscopy Sciences) and staining with a freshly prepared 2% uranyl formate solution for 0.5 min.

smFRET characterization of DNA walkers on DNA nanostructures. Microscope slides with a flow channel were prepared using double-sided tape (3M) and treated with biotinylated BSA and streptavidin as previously described[32,33] to prepare the surface for immobilization of biotinylated DNA nanostructures. DNA tile or origami (15 µl of a 10 nM solution) and DNA walker (10 µl of a 10 nM solution) were combined and incubated in the dark at 37 °C for 5 min. This mixed sample was diluted to 20 pM in TA-Mg^{2+} buffer (40 mM Tris, 20 mM acetic acid and 12.5 mM magnesium acetate, pH 8.0), then injected into the flow chamber. After incubating for 10 min, TA-Mg^{2+} buffer was injected to remove excess unbound material.

Single-molecule FRET experiments were carried out on an inverted prism-type TIRF microscope with a 1.2 NA ×60 water-immersion objective (IX71, Olympus) in a darkened room at an environmentally controlled temperature of 20 ± 3 °C. Fluorescence excitation was provided by a 532-nm green laser (CrystaLaser CL532-050-L, 50 mW, attenuated and focused to give an illumination intensity of ~100 W cm^{-2} in the sample plane). The presence of an active FRET acceptor was confirmed at the beginning of each experiment by brief excitation with a 640-nm red laser (Coherent CUBE 635–25C, 25 mW). The Cy3 and Cy5 emission signals were separated by a dichroic mirror with a cut-off wavelength of 610 nm (Chroma) and projected side-by-side onto an ICCD camera chip (iPentamax HQ Gen III, Roper Scientific) with a full-frame acquisition rate of 10 Hz. The Cy3 channel image was passed through a bandpass filter (HQ580/60m, Chroma) and the Cy5 channel was passed through a long-pass filter (HQ655LP, Chroma). A Newport ST-UT2 vibration isolation table was used in all experiments to reduce instrument interference. In all smFRET measurements, an oxygen scavenger system (OSS; 5 mM 3,4-dihydroxybenzoic acid, 2 mM Trolox, and 50 nM protocatechuate dioxygenase) was included in the imaging buffer to retard photobleaching[16,34].

Analysis of smFRET trajectories was performed with custom-written MATLAB scripts as previously described[35], with the FRET ratio at each time point calculated as $I_{Cy5}/(I_{Cy5}+I_{Cy3})$, where I_{Cy5} and I_{Cy3} are the apparent fluorescent intensities of Cy5 and Cy5, respectively. A given smFRET trajectory was used in subsequent analyses only if the following conditions were met: it exhibited total fluorescence of Cy3 and Cy5 exceeding 500 counts per frame; it showed clear evidence of both Cy3 and Cy5 fluorescence; and it showed no evidence of multiple identical fluorophores, for example, multiple photobleaching steps or overlapping point-spread functions in the CCD image. After trajectories that met the criteria were selected, Hidden Markov modelling was applied using the QuB software suite (State University of New York at Buffalo, USA) to determine the mean dwell times in high- and low-FRET states for each trajectory[36]. The same two-state model was applied to all datasets. After idealization, the dwell times in the high- and low-FRET states (red and blue lines, respectively, in Fig. 2f–i) were extracted from each trace, and the mean value of all high-FRET, low-FRET or (high-FRET + low-FRET) dwell times were used to describe the mean dwell time of each molecule. These mean dwell times across all observed molecules are represented as box-and-whisker plots in Fig. 2n–o. Transition occupancy density plots, which depict the fraction of molecules among all molecules characterized that transition from a specific initial FRET state to a different (final) FRET state at least once, were constructed from the idealized data as described previously[35].

Cross-correlation between donor and acceptor fluorescence signal (Fig. 1e) was calculated using the built-in MATLAB function xcorr with unbiased normalization. The cross-correlation signal was further normalized such that the cross-correlation approaches 0 at infinite time lag, and any positive or negative correlation is confined to the interval [−1,1]. The decay time of cross-correlation was estimated by a single-exponential fit.

Preparation and characterization of high-density foothold-functionalized surfaces. Coverslips (22 × 50 mm) were sonicated in a solution of 2% Alconox for 5 min and then rinsed five times with deionized water. Rinsed coverslips were incubated in heated base piranha solution (5% hydrogen peroxide and 5% ammonium hydroxide, 60–70 °C) for 40 min. Coverslips were rinsed five times with deionized water and then once with ethanol, and dried under an air stream. Dry coverslips were placed into a box with ethanol-soaked Kimwipes (Kimberly Clark). A 2% silane solution was prepared by combining 2 µl 11-azidoundecyltriethoxysilane and 98 µl ethanolic acetic acid (95% ethanol plus 5% aqueous acetic acid), and 80 µl of the solution was added to the coverslip. Another coverslip was placed on top to form a sandwich. After a 10-min incubation, the coverslip sandwiches were flipped over and incubated for a further 10 min. After a total 20-min incubation, the coverslips were rinsed with absolute ethanol twice and dried under air.

Amine-modified oligonucleotides ($F_{1,covalent}$: 5′-CAATACCCCTAC GGTCACTTCTTTTTTTTTT/3AmMO/; and $F_{1,covalent}$: 5′-/5AmMC6/ TTTTTTTTTTCCCTCATTCAATACCCCTACG) were functionalized with dibenzocyclooctyne (DBCO) as follows: DMF (200 µl) and DBCO-NHS ester (5 mg) were combined to prepare a 62.5 mM solution of DBCO-NHS ester. A volume of amine-modified foothold strand F_1 or F_2 (20 µl of 1 mM aqueous solution) was combined with DBCO-NHS ester (40 µl of 62.5 mM solution), DMF (39 µl) and TEA (1 µl) and incubated for 2 h at room temperature. DNA was precipitated by adding sodium acetate (10 µl, 3 M) and chilled 100% ethanol (200 µl) to the reaction, and incubating at −20 °C for 30 min. The precipitated DNA was pelleted by centrifugation at 20,000 × *g*, 4 °C, for 40 min. The supernatant was removed, and the precipitate was rinsed with 80% ethanol (100 µl) and spun down again for 1 min. The supernatant was again removed, and the pellet was dried in a vacufuge for 10 min. A UV spectrum was collected to measure the concentration of DBCO-functionalized oligonucleotides. The absorbance of DBCO at 310 nm was used to estimate the ratio of DBCO to DNA (approximately 1:1) after subtracting the absorbance of the DNA at 310 nm based on its absorbance at 260 nm and the extinction coefficients at 260 and 310 nm predicted using the UV Spectrum application from IDT Biophysics.

Click conjugation of oligonucleotides to azide-functionalized coverslips was performed as follows. Solutions of 50 µM DBCO-functionalized foothold oligonucleotides F_1 and F_2 were prepared in PBST buffer (1× PBS + 0.1% Tween-20). Equal volumes of each 50 µM oligonucleotide solution were combined, and 1 µl of the mixture was spotted onto the 11-azidoundecyltriethoxysilane-modified coverslips. The click reaction proceeded overnight for more than 15 h in a humid environment. Coverslips were rinsed thoroughly using deionized water for more than 10 s and dried under N_2.

The density of click-conjugated oligonucleotides on coverslip surfaces was estimated as follows. For purposes of density characterization, only DBCO-modified F_1 strands were added (at 50 µM) during the click conjugation. After constructing the sample wells (see Single-particle tracking and data analysis, below), 100 µl of a mixture containing 1 pM Cy5-labelled $W_{8\_13\_8}$ and 1 µM (1-million-fold excess) of a non-fluorescent $W_{8\_13\_8}$ in TA-Mg^{2+} buffer was added to the sample well and incubated for 10 min. The solution was replaced by 100 µl of OSS and the sample was imaged on the same TIRF microscope used for single-particle tracking, under illumination at 640 nm. The number of Cy5-labelled walker molecules bound within each field of view was estimated using a custom MATLAB script, and averaged over 23 fields of view, and multiplied by 10^6 to estimate the total number of labelled and unlabelled $W_{8\_13\_8}$ molecules per field of view, $n = 3.0 \times 10^8$. For each field of view, the area is $S = (262\,\text{nm per pixel} \times 512\,\text{pixels})^2 = 17{,}990\,\mu\text{m}^2$. The density of foothold oligonucleotides is $n/S = 1.67 \times 10^4\,\mu\text{m}^{-2}$.

To estimate the typical distance to the nearest available foothold of the opposite type (since a walker with a dissociated toehold domain can step only onto F_1 if it is bound to F_2, and vice versa), we performed numerical simulations of the distribution of footholds F_1 and F_2 in two dimensions (Supplementary Fig. 8). We assumed an independent uniform random distribution of each foothold on the surface and the same density of footholds as we observed experimentally ($1.67 \times 10^4\,\mu\text{m}^{-2}$; in the simulation, this translates to 8,350 copies of F_1 and 8,350 copies of F_2 in a 1,000 nm × 1,000 nm region). We then calculated the distance to the nearest F_2 for each foothold F_1, and plotted a histogram of these distances (Supplementary Fig. 8). This simulation predicts that the mean distance to the nearest foothold is 5.5 nm, and > 98.5% of footholds will have at least one foothold of the opposite type within 13 nm.

Estimation of mean step size in 2D walking experiments. To estimate the mean step size, we approximated the mean distance between the anchor point of the foothold and the distal (free) toehold of the walker as (length of walker–foothold duplex) + (length of single-stranded linker between the coverslip and walker). The length of the walker–foothold duplex was calculated as (number of nucleotides) × (0.332 nm per nucleotide). The RMS end-to-end distance of the single-stranded linker (dT_{10} + any unpaired toehold nucleotides in the proximal foothold) was estimated using a freely jointed chain model according to the formula $\text{RMSD} = \sqrt{Nl}$, where N is the number of Kuhn segments and l is the persistence length[37], assuming a persistence length of 1.5 nm and a contour length of 0.56 nm per nucleotide[38]. The step sizes of the two walkers used in single-particle tracking were estimated as 10.8 nm (for $W_{6\_13\_6}$) and 11.1 nm (for $W_{8\_13\_8}$), which were used in generating the simulated mean square displacement (MSD) versus time traces for Fig. 3f. However, given the predicted contour length of the 10–12 nucleotide ssDNA linker (5.6–6.7 nm) and the predicted length of the 19–21 nucleotide dsDNA segment (6.3–7 nm), the maximum end-to-end distance of each walker may be as large as 12.5–13 nm.

Single-particle tracking and data analysis. A 200-µl Eppendorf micropipet tip was cut with a razor blade and attached to the F_1 and F_2 modified coverslip by Epoxy (Double Bubble, Hardman Adhesives) as previously described[39] to form a sample chamber with the DNA-coated region positioned approximately in the centre of the chamber. The sample chamber was incubated with 100 µl PBST buffer (1× PBS + 0.1% Tween-20) for 10 min, then for 15 min with a 100 µl mixture containing 1 pM DNA walker and 10 pM Cy3-labelled fiducial marker oligonucleotide (sequence fully complementary to F_1) in PBST. The walker sample was then removed and the chamber was rinsed three times before imaging.

Single-particle tracking experiments were performed on an Olympus IX-81 objective-type TIRF microscope equipped with a ×60 oil-immersion objective (APON ×60 OTIRF, 1.49 NA) with both Cell^TIRF and z-drift control (ZDC2) modules, and an EMCCD camera (IXon 897, Andor, EM gain 300). Cy5 excitation was provided by a 640-nm red laser (Coherent CUBE 640–100C, 100 mW) and Cy3 excitation was provided by a 532-nm green laser (CrystaLaser CL532-150-L, 150 mW). In all single-particle tracking experiments, an OSS was included in the imaging buffer to retard photobleaching. The translocation of DNA walkers was monitored under alternating TIRF excitation at 640 and 532 nm (time lapse interval of 30 s, exposure time of 100 ms) for 60 min.

Analysis of single-particle tracking experiments was performed as follows. The ImageJ plug-in Particle Track and Analysis (PTA) was used to conduct 2D Gaussian fitting by the Levenberg–Marquardt method to obtain trajectories for each detected walker molecule[40]. The search area was set to 3 pixels (= 402 nm). The net movement of all fiducial markers in the field of view was subtracted from walker trajectories using a custom MATLAB script to account for x–y stage drift. A given trajectory was used in subsequent analysis only if the following conditions were met: lasted 10 min (20 frames) without photobleaching; exhibited no sudden fluorescence intensity changes as determined by manual inspection of the output from PTA fitting; and showed no evidence of multiple identical fluorophores, such as multiple photobleaching steps or overlapping point-spread functions in the CCD image.

Calculation of MSD was performed as follows. An initial position (x_0, y_0) was defined as the arithmetic mean of the first three position measurements of each trajectory. The distance of each subsequent position measurement (x_i, y_i) from the initial position (x_0, y_0) was then calculated and squared to obtain the squared net displacement over time. The arithmetic mean of the MSD was calculated for all trajectories lasting at least 10 min, and the corresponding standard error (S.E.) of the mean was calculated for each MSD value as plotted in Fig. 3f. After fitting a linear function to each MSD versus time plot in OriginPro 8.0, the slope of the linear fit was divided by 4 to obtain the apparent 2D diffusion coefficient (D) for each walker, based on the 2D diffusion model $(x(t))^2 = 4Dt$. The diffusion coefficient was also predicted from smFRET measurements of stepping kinetics using the 2D random walk model $(\Delta x)^2 = 4D\Delta t$, where Δx is the step size and Δt is the mean stepping lifetime of a representative (median-valued) walker.

Kinetic Monte Carlo modelling of branch migration and stepping kinetics in a three-foothold system. The branch migration and stepping of walkers in a three-foothold system was numerically simulated at single-base resolution using a version of the Gillespie algorithm[41] implemented in MATLAB. Additional details regarding the simulations and their interpretation are provided in Supplementary Note 1. Autocorrelation of the branch migration state was calculated as a function of time lag using the xcorr function in MATLAB, and normalized in the same manner as for cross-correlation in the smFRET data.

Data availability. The data that support the plots within this paper and other findings of this study are available from the corresponding author upon reasonable request.

References

32. Ha, T. Single-molecule fluorescence resonance energy transfer. *Methods* **25**, 78–86 (2001).
33. Michelotti, N., de Silva, C., Johnson-Buck, A. E., Manzo, A. J. & Walter, N. G. A bird's eye view tracking slow nanometer-scale movements of single molecular nano-assemblies. *Methods Enzymol.* **475**, 121–148 (2010).
34. Aitken, C. E., Marshall, R. A. & Puglisi, J. D. An oxygen scavenging system for improvement of dye stability in single-molecule fluorescence experiments. *Biophys. J.* **94**, 1826–1835 (2008).
35. Blanco, M. & Walter, N. G. Analysis of complex single-molecule FRET time trajectories. *Methods Enzymol.* **472**, 153–178 (2010).
36. Nicolai, C. & Sachs, F. Solving ion channel kinetics with the qub software. *Biophys. Rev. Lett.* **08**, 191–211 (2013).
37. Dill, K. A. & Bromberg, S. Molecular Driving Forces: Statistical Thermodynamics in Chemistry and Biology. (Garland Science: New York, 2003).
38. Chen, H. et al. Ionic strength-dependent persistence lengths of single-stranded RNA and DNA. *Proc. Natl Acad. Sci. USA* **109**, 799–804 (2012).
39. Johnson-Buck, A. et al. Kinetic fingerprinting to identify and count single nucleic acids. *Nat. Biotechnol.* **33**, 730–732 (2015).
40. Particle Track and Analysis (PTA) (Yoshiyuki Arai, accessed 29 August 2017); http://www.sanken.osaka-u.ac.jp/labs/bse/ImageJcontents/frameImageJ.html
41. Gillespie, D. T. Exact stochastic simulation of coupled chemical reactions. *J. Phys. Chem.* **81**, 2340–2361 (1977).